Int. J. Heat Mass Transfer. Vol. 30, No. 6, pp. 1183–1192, 1987
Printed in Great Britain

0017-9310/87 $3.00+0.00
© 1987 Pergamon Journals Ltd.

Mass transfer in a three-dimensional net-type turbulence promoter

WOO SIK KIM, JOONG KON PARK† and HO NAM CHANG‡
Department of Chemical Engineering, Korea Advanced Institute of Science and Technology,
P.O. Box 131 Chongyang, Seoul, Korea

(*Received* 31 *July* 1985 *and in final form* 10 *October* 1986)

Abstract—Local mass transfer rates in a three-dimensional net-type turbulence promoter were measured using a limiting current technique and flow patterns were visualized with an ink tracer. The model promoter consisted of upper and lower rectangular flow channels which overlapped at a given angle to form an interfacial contacting and mixing region for the two layers of fluid streams coming through each channel. Local and overall mass transfer rates using 16 segmented electrodes were measured to study the effects of the Reynolds number (*Re*) and the ratio of two average velocities in the lower and upper channels by varying cross flow angle and the ratio of channel height to width. The highest mixing efficiency was obtained in the promoter with 135° cross flow angle and progressively less in those with 90° and 45° cross flow angles. Flow visualization showed that in the three-dimensional promoter a vortex created by two interfacial cross flows was the main mechanism in breaking a concentration boundary layer in contrast to the recirculating flows in the two-dimensional promoters studied by Chang and co-workers (1983, 1984).

1. INTRODUCTION

IN A LIQUID–solid mass transfer system such as electrodialysis it is important to understand the nature of the transfer of a transfer limiting step. When mass transfer is limited by the diffusion in the concentration boundary layer near the membrane, the mass transfer resistance is proportional to its thickness which grows along the flow path and also is heavily influenced by the flow regime. In order to increase the mass transfer rate a turbulence promoter has often been employed. This promoter serves as a membrane support and, more importantly, facilitates mixing in the boundary layer. As a result, the growth of the concentration boundary layer is blocked and mass transfer rate is enhanced by a recirculating flow between the promoters.

Because of the complexity of flow in the system it has been common practice to simplify the system to a two-dimensional model. Miyashita *et al.* [1] and Watson and Thomas [2] carried out mass transfer studies on the attached and the detached cylindrical promoter. Solan *et al.* [3] proposed a simple analytical 'mesh step model' to study the spacer performance. In their model, 'the mesh size' characterized the spacer and 'the mixing efficiency' described the partial mixing of the concentration profile at each step. Belfort and Guter [4] studied the hydrodynamic performance of various spacers in electrodialysis and suggested the criteria for evaluating the spacer. They also showed that the spacers were influenced very differently from one another because of their complexity of design and variation in construction materials and flexibility. The hydrodynamic performance of zig-zag and cavity type two-dimensional spacers was analysed numerically as well as experimentally by Chang and co-workers [5, 6]. All previous studies were recently reviewed by Chang and Park [7].

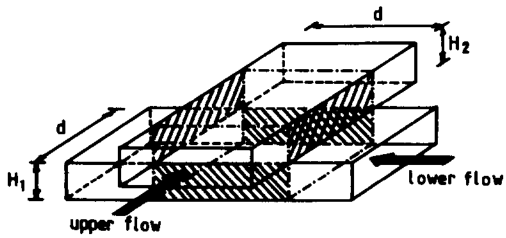

FIG. 1. Modelled system for a three-dimensional turbulence promoter.

A three-dimensional net-type turbulence promoter, which has been used in an electrodialysis process, has a very different mixing mechanism from that of a two-dimensional unit. The promoter has two layers of fluid streams coming from different directions, which are to contact and mix in the chamber to create a radial as well as a vertical recirculation (Fig. 1). The present investigation aims at the experimental study of mass transfers in the cross flow region by varying the Reynolds number (*Re*) and the geometry of the three-dimensional promoter. The results will be compared with those of two-dimensional ones and those in a straight flow duct without the upper cross flow.

2. EXPERIMENT

2.1. *Limiting current method*

The limiting current method is most widely used in measuring the mass transfer between a solid surface

† Present address: Kyungpook National University.
‡ To whom all correspondence should be addressed.

NOMENCLATURE

C_b bulk concentration
C_s concentration at a solid surface
C_j concentration of j-component
D diffusivity
d width of the flow channel and the characteristic length in the promoter
F Faraday's constant (96,487 Coulomb $equiv^{-1}$)
GP1 geometric parameter meaning the ratio of the height to the width of the lower channel (H_1/d)
GP2 geometric parameter meaning the ratio of the average velocities in the upper and the lower flow channels ($U_{upper}/U_{lower} = H_1/H_2$)
H_1 height of the lower flow channel
H_2 height of the upper flow channel
i current density
i_{lim} limiting current density
k mass transfer coefficient
N_j mass flux of j-component
Re Reynolds number ($U_{lower}d/\nu$)
Sh Sherwood number (kd/D)
X, Y normalized distance along and perpendicular to the flow direction in a straight flow duct
z_j number of ions of j-species exchanged during electrochemical reaction.

Greek symbols
ν kinematic viscosity
θ cross angle of flow channels.

Subscripts
L local
m mean
x area averaged along Y-direction.

Superscripts
a, b, c exponents of Re, GP1 and GP2, respectively.

and an adjacent liquid layer. With the assumption that electrical and convective transports are negligible compared to diffusive transport [8, 9], the mass flux equations become

$$N_j = k_j(C_b - C_s) \quad (1)$$

where k_j is the mass transfer coefficient and C_b and C_s are concentrations of the j-component in the bulk and on the surface of the electrode, respectively. From the measured current 'i' k_j is obtained as

$$k_j = i/z_jF(C_b - C_s) \quad (2)$$

where F is the Faraday constant. In the limiting current situation C_s is zero. Thus equation (2) becomes

$$k_j = i_{lim}/z_jFC_b. \quad (3)$$

From equation (3) we can deduce the dimensionless mass transfer rate, Sherwood number, Sh as

$$Sh = k_jd/D_j = i_{lim}d/z_jFC_bD_j \quad (4)$$

where d is the characteristic length and represents the channel width in this system. We used a limiting current system of 0.01 M potassium ferricyanide and ferrocyanide dissolved in 1 M NaOH. The details of the procedure were described previously [10].

2.2. *Experimental system*

A schematic diagram of the experimental system is shown in Fig. 2. The test cell (1) simulating a single mesh in net-type turbulence promoters consisted of two rectangular flow channels which simply overlapped each other at a given angle. The upper and lower plates of the test cell were made of 10 mm thick lucite and the side walls were rubber sheets 2.5 and 5 mm in thickness. The test cell shown in Fig. 1 had four open side walls, two of which were located in the lower channels and the other two in the upper channel. Thus the fluid streams coming from each channel meet in the cell.

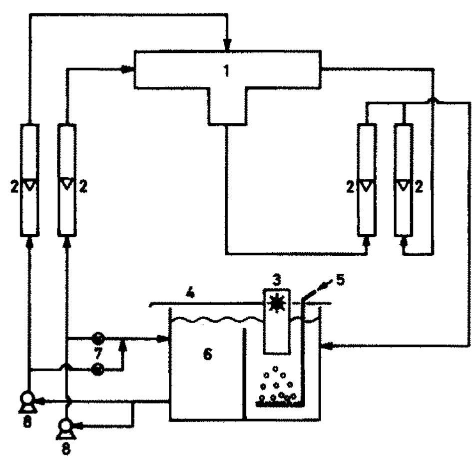

FIG. 2. A schematic diagram of experimental systems: 1, test cell; 2, flow meters; 3, temperature controller; 4, cover; 5, nitrogen gas; 6, tank; 7, bypass valve; 8, pump.

The cathode package arranged in a 4×4 matrix type was installed in the cross flow region of the lower plate of the test cell and a large anode, 20 mm wide and 100 mm long, was installed at the downstream end of the lower plate to ensure the oxidation of ferrocyanide. All the electrodes were made of nickel. In the 90° cross angle case the cathode package was

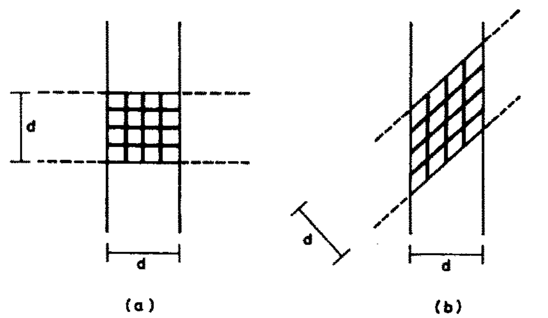

FIG. 3. Arrangement of cathodes: (a) $\theta = 90°$; (b) $\theta = 45°$, 135°.

made of 16 rectangular nickel plates of 4.52 × 4.52 mm area, which were arranged in 2 × 2 cm area as in Fig. 3(a). In the case of 45° and 135° cross angles the cathode package was made of 16 parallelogram nickel plates of 4.50 × 6.41 mm area as in Fig. 3(b).

Epoxy resin was used to ensure electrical isolation and fix the cathodic electrodes. The cathodes and epoxy resin played the roles of active and inert regions, respectively, and the ratio of the active region to the total surface area was 0.81. Since the surface condition of the electrode had a significant influence on the limiting current, the surface was polished with fine emery papers, No. 1200, No. 1500 and No. 2000 in turn, to remove any oxide film and washed with carbon tetrachloride to remove oil film. In order to activate the electrodes, cathodic treatment was performed by placing electrodes in 2 M NaOH solution and applying a negative potential for 5 min.

The direct voltage of 0.65 V was constantly applied by the d.c. power supply and the supplied voltage and the current were measured by digital multimeters, respectively. When the currents fluctuated, they were made to pass through a 120 Ω resistor and the voltage across the resistor was recorded by a dual-pen chart recorder.

2.3. *Experimental procedure*

In order to remove dissolved oxygen in the solution nitrogen was bubbled at 3 l min^{-1} for 2 h before the experiment and bubbling continued during the experiment. The solution reservoir was painted black to prevent decomposition of ferrocyanide owing to light. The solution was pumped to the test cell by the two micropumps. The disturbance was minimized by the bypass line and the flow rate was controlled by the control valve. The temperature of the solution was kept at 25°C. The concentrations of ferricyanide and ferrocyanide were measured by the iodometric method [11] and by permanganate titration [12].

3. RESULTS AND DISCUSSION

In order to see the effects of the geometry and the Reynolds number on the mass transfer we have defined three dimensionless variables: *Re*, $U_{lower}d/\nu$ where U_{lower} is the velocity in the lower channel and d is the width of the channel; GP1, the ratio of the height to the width of the lower channel (H_1/d); GP2, the ratio of the upper velocity to that of the lower flow (U_{upper}/U_{lower}). Here not d or ν. Since the flow in the upper and lower channels was made the same, GP2 also reflected the ratio of the lower channel height to the upper channel height (H_1/H_2).

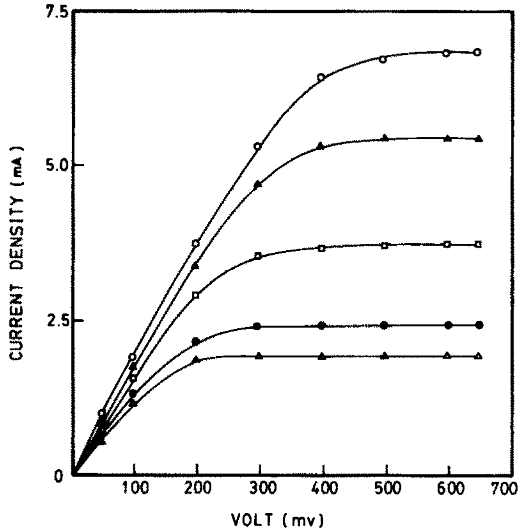

FIG. 4. Polarization curve for the reduction of ferricyanide (GP1 = 0.25, GP2 = 1.0, $\theta = 90°$ and $Sc = 1650$): ○, $Re = 2400$; ▲, $Re = 1600$; □, $Re = 800$; ●, $Re = 400$; △, $Re = 200$.

Prior to measurement of the local mass transfer rate, polarization curves were obtained as shown in Fig. 4. The limiting current increased with *Re*, which is explained by the thinner mass transfer boundary layer at the higher Reynolds number.

Figure 5 shows the local Sherwood number, Sh_L, distributions in a straight flow duct at $Re = 800$, GP1 = 0.5 for a rectangular cathode (Fig. 3(a)) and a parallelogram cathode (Fig. 3(b)). The local Sherwood number, Sh_L, decreased due to the development of the concentration boundary layer as X increased. While Sh_L was proportional to $X^{-1/3}$ in the fully developed two-dimensional laminar flow between flat plates, Sh_L in the straight flow duct also changed with Y-position as well as X-position because of the side wall effect. The maximum Sh_L occurred at the centre of the inlet electrode. Here the local mass transfer rates in Fig. 5(b) were lower than those in Fig. 5(a), but there was little difference between the two shapes of the distributions. As shown in Fig. 3, the mass transfer area and length of the electrode in Fig. 3(b) were about 41% larger than those in Fig. 3(a). By this reason the mass transfer rate per unit area at each electrode in Fig. 5(b) was less by 20% than that in Fig. 5(a). Assuming that the mass transfer is of Leveque type in two-dimensional flow, the area averaged mass transfer of the parallelogram electrode should be 12% less than that of the rectangular electrode. This discrepancy between the theoretical decrease and the real measured decrease in two cases

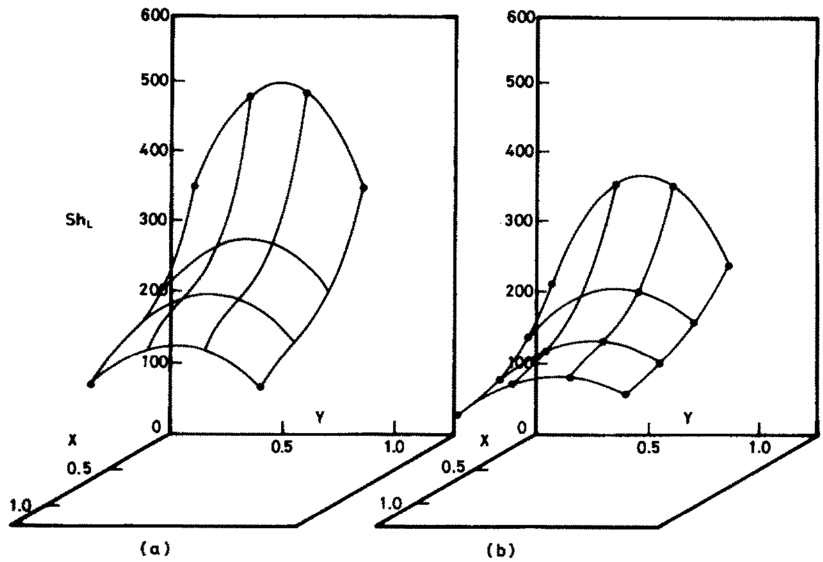

FIG. 5. Local Sherwood number distribution in a straight flow duct ($Re = 800$, GP1 = 0.5): (a) cathodes arranged as in Fig. 3(a); (b) cathodes arranged as in Fig. 3(b).

of electrode shapes seems to originate from the side wall effect of the flow duct. Even though the local mass transfer rate in the straight flow duct changed with Re and GP1, there was little difference in the overall shapes of the distribution.

Figure 6 shows the local mass transfer rate, Sh_L, at each cross flow (45°, 90° and 135°) of GP1 = 0.25, GP2 = 2.0 and $Re = 400$. All have different Sh_L profiles than those in Fig. 5. In the 45° cross flow the lower flow may not deviate from the laminar flow regime because the shear force exerted by the upper flow is somewhat in the same direction as the lower flow. So the Sh_L distribution was not so much deformed from that in the straight flow duct. But Sh_L near the wall of $Y = 1.0$ was higher than that near the wall of $Y = 0$ since the lower flow channel acted on the upper flow like the cavity type promoter. This phenomena was more pronounced in the 90° cross flow and was consistent with Kim *et al.*'s result [6] in the two-dimensional cavity type promoter. In the 135° cross flow the Sh_L distribution was more complicated due to the shear force and mixing effect exerted by the upper flow. Therefore, the differences between distribution shapes of the straight duct flow and the cross flow stemmed from that the local mass transfer rate was heavily influenced by the cross angle. That is, the larger cross angle creates the higher degree of mixing and turbulence flow in the chamber, which results in a wide fluctuation of local mass transfer rates. To visualize the cross flow pattern tracer studies were performed (Fig. 7). In the 45° cross flow the flow paths of the tracers injected at positions 1, 2 and 3 were undisturbed by the upper flow, but the tracer injected at position 4 was influenced slightly by the upper flow (Fig. 7(a)). In the 90° cross flow the tracer injected at position 4 was completely diverted to the upper flow direction (Fig. 7(b)). In the 135° cross flow the tracers at all positions were diverted to the upper flow direction (Fig. 7(c)). This partially explains the abnormal behavior of Sh_L at the three-dimensional cross flow type promoters which is completely different from that in a straight flow duct. These photographs show no flow separation around the turbulence promoter, which suggests that the recirculating flow is not a main mechanism in this mass transfer promotion.

The effect of Reynolds number on the local Sherwood number averaged along the Y-direction, Sh_x, in each cross flow is shown in Fig. 8 for GP1 = 0.25 and GP2 = 1.0. The effect is less pronounced in the 45° cross flow, but it is highly contrasted to that in the 135° cross flow. It is interesting to note that Sh_x increases with X in contrast to that in a straight duct flow shown in Fig. 5 and those in the smaller angle cross flows. This is mainly due to the mixing effect, which was shown in the tracer study. Distributions of Sh_x for GP1 = 0.125 and GP2 = 2.0 are shown in Fig. 9, which are considerably different from those in Fig. 8. The Sh_x distribution in the 45° cross flow had a minimum value point at $X = 0.375$ at the high Reynolds number in contrast to that in Fig. 8(a). In the 90° cross flow the minimum value point also appeared and this point shifted from $X = 0.625$ to 0.375 as Reynolds number increased. This phenomena may be due to the increase of the contribution of the shear force to the lower flow. That is, the shear force exerted by the upper flow created the vortex in the lower flow and increased the magnitude of the velocity around the lower plate. Since the lower flow channel acted on the upper flow like the cavity, this contribution of the shear force to the velocity distribution around the lower plate increased as the depth of the lower flow channel decreased. Adversely, Fig. 10 shows Sh_x distributions with the increased depth of the lower flow

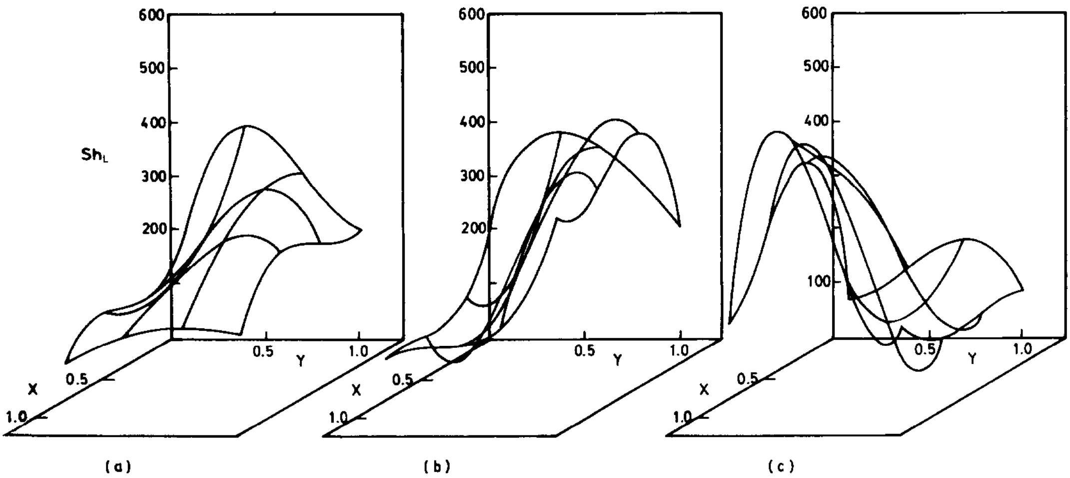

FIG. 6. Local Sherwood number distribution (Re = 400, GP1 = 0.25, GP2 = 2.0): (a) $\theta = 45°$; (b) $\theta = 90°$; (c) $\theta = 135°$.

channel, which means that the contribution of the shear force to the velocity distribution around the lower plate is reduced. The effect of the depth of the lower flow channel was clearly pronounced in the Sh_x distribution of the 45° cross flow because the mass transfer in the smaller angle cross flow would be promoted mainly by the shear force rather than by the mixing effect, but was the reverse of that of the 135° cross flow because the mass transfer would be promoted mainly by the mixing effect rather than by the shear force. This effect of the depth on the velocity distribution was shown in two-dimensional cavity flows by Torrance *et al.* [13] and so we could infer from Sh_x distributions in the smaller angle cross flow that our expectation was in fair agreement with their work. Pan and Acrivos [14] also showed in two-dimensional cavity flows that the velocity on the bottom plate decreased as the depth of the cavity increased and then insisted that the viscous force increased to the comparable magnitude with the inertia force as the depth of the cavity became infinite.

Figure 11 shows Sh_x distributions for GP1 = 0.25 and GP2 = 0.5. Since the upper flow rate was half of the lower flow rate, the upper flow had a less effect on the lower flow, relatively. In comparison with Fig. 8 it could be readily found that the mass transfer rates in Fig. 11 were less promoted. The Sh_x distribution in the 135° cross flow had a minimum value at $X = 0.375$ with $Re = 800$. This indicates that the mixing effect on the mass transfer rate becomes small as the upper flow rate decreased. Figure 12 shows Sh_x distributions for GP1 = 0.25 and GP2 = 2.5, which mean implicitly the increase of the shear force and the mixing effect. The mass transfer rate was promoted with the faster upper flow rate. And then in the 45° cross flow this resulted in the more increased Sh_x distribution without a minimum value point, which was different from those in the other situations. These results from Figs. 8, 11 and 12 confirm that the upper flow rate has influence on the mass transfer rate in all cross angles.

Therefore, it can be deduced from Figs. 6–12 that the pattern of the local Sherwood number distribution is more dependent on the cross angle. That is, we can say that the mass transfer promotion in the smaller cross angle results primarily from the shear force exerted by the upper flow and that the mass transfer promotion in the larger cross angle results primarily from the mixing effect in the cross chamber.

Figure 13 shows the effect of Reynolds number on the mean Sherwood number, Sh_m, for each cross flow. As seen in the cases of the local Sherwood number, the slope is steeper in the larger angle cross flow.

Figure 14 shows the correlations between the mean Sherwood number and parameters, Re, GP1 and GP2, at each cross angle. The correlations are

$$Sh_m = 15.78 Re^{0.399}\,\mathrm{GP1}^{-0.193}\,\mathrm{GP2}^{0.207} \qquad \theta = 45°$$

$$Sh_m = 14.42 Re^{0.475}\,\mathrm{GP1}^{-0.042}\,\mathrm{GP2}^{0.177} \qquad \theta = 90°$$

$$Sh_m = 5.82 Re^{0.661}\,\mathrm{GP1}^{0.212}\,\mathrm{GP2}^{0.220} \qquad \theta = 135°.$$

In these correlations the mean Sherwood number is dependent on Reynolds number as strongly as the cross angle increased. In the 45° cross flow the flow regime does not seem to deviate from the laminar flow regime and furthermore the dependency of Sh_m on Re is nearly consistent with that in two-dimensional flow between flat plates. As seen in the tracer study, the amount of mixing of the two flows in the cross chamber increased with the cross angle. Thus, the exponent of Re in the Sh_m correlation also increased with the cross angle because the cross flow became the turbulence flow by the stronger mixing effect. As GP2 increased, Sh_m also increased. But the effect of GP1 was rather mixed. In the 45° cross flow the exponent is negative, which means that the smaller GP1 yields the higher Sh_m. In other words, a thinner flow channel is more effective in increasing the mass transfer. But in the 135° cross flow the effect is reversed because the mass transfer is promoted mainly by the mixing effect. The mixing effect seems to reflect the complicated nature of the mixing mechanism in this promoter.

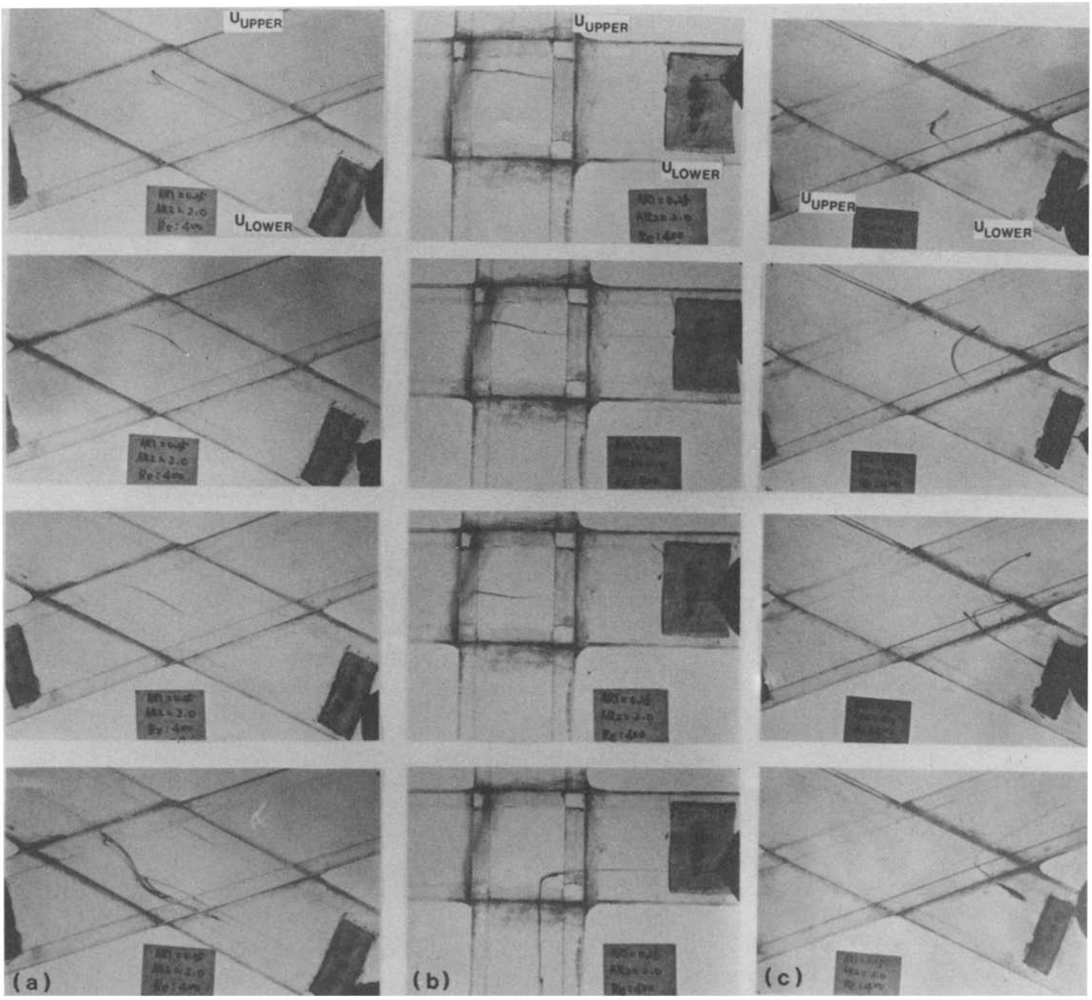

FIG. 7. Tracer study of flow path. The conditions are the same as in Fig. 6: (a) $\theta = 45°$; (b) $\theta = 90°$; (c) $\theta = 135°$. The injection point moves along the upper flow direction. Flow directions are denoted by U_{upper} and U_{lower}.

In Table 1 Sherwood numbers in the two-dimensional zig-zag promoter by Kim *et al.* [6] and the straight flow duct were compared with the results of the present study. The three-dimensional cross flow promoters were superior to any of the two-dimensional promoters.

4. CONCLUSIONS

A three-dimensional turbulence promoter works more effectively than a two-dimensional turbulence promoter in breaking the concentration boundary layer and increasing the mass transfer rate. Flow visu-

Table 1. Comparison of Sherwood numbers among the turbulence promoters

Re	2-D zig-zag promoter AR = 5	3-D cross flow promoter GP1 = 0.125, GP2 = 1.0			2-D straight duct flow GP1 = 0.125	
		45°	90°	135°	45°, 135°	90°
100	54.8	64.4	67.7	49.1	50.5	64.3
200	71.2	84.9	94.1	77.7	62.8	87.7
400	92.4	111.9	130.9	122.8	86.7	110.4
800	119.9	147.5	181.9	194.2	116.9	143.9
1200	139.6	173.4	220.5	253.9	139.9	165.2
	Kim *et al.* [6]		This study		This study	

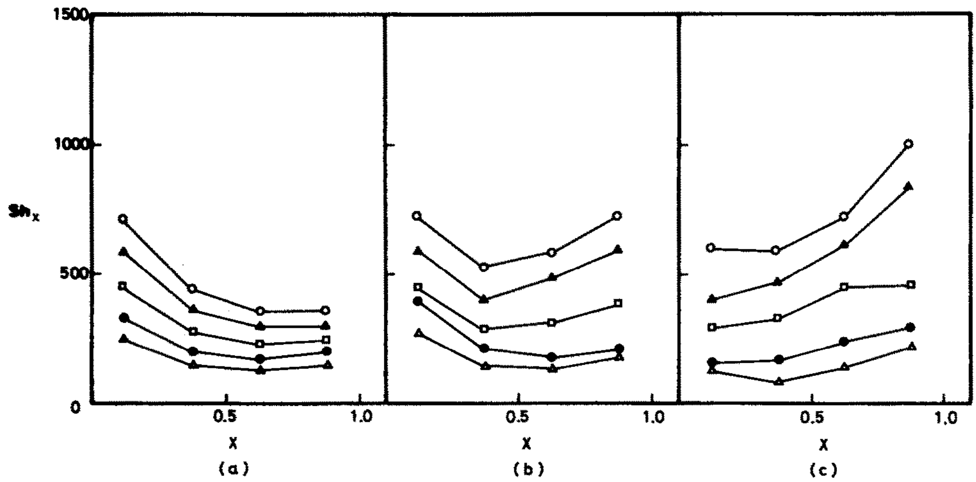

FIG. 8. Local Sherwood number distribution (GP1 = 0.25, GP2 = 1.0): (a) $\theta = 45°$; (b) $\theta = 90°$; (c) $\theta = 135°$. The symbols are the same as in Fig. 4.

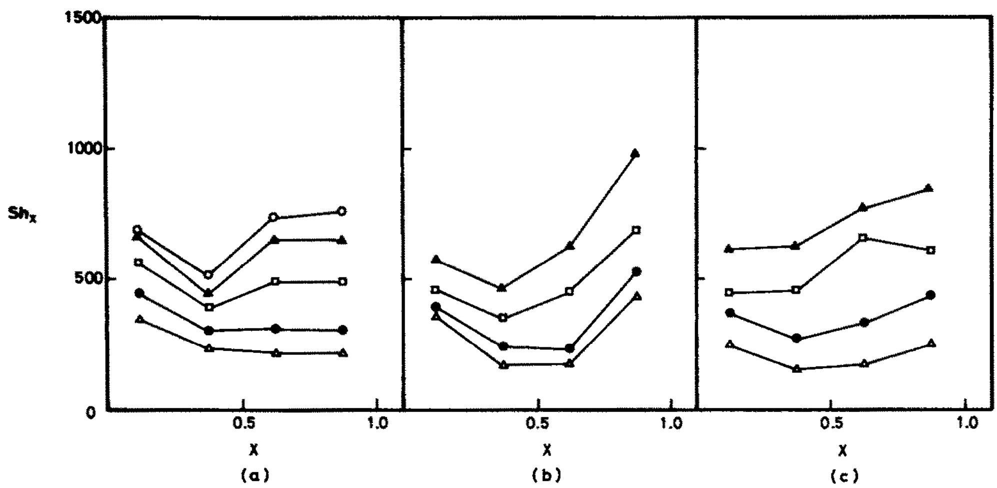

FIG. 9. Local Sherwood number distribution (GP1 = 0.125, GP2 = 1.0): (a) $\theta = 45°$; (b) $\theta = 90°$; (c) $\theta = 135°$. ○, $Re = 4800$; ▲, $Re = 3200$; □, $Re = 1600$; ●, $Re = 800$; △, $Re = 400$.

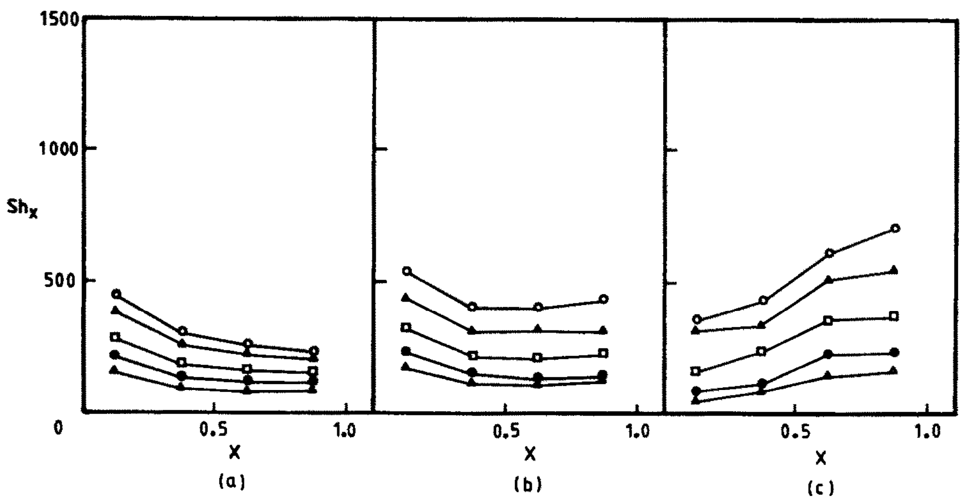

FIG. 10. Local Sherwood number distribution (GP1 = 0.5, GP2 = 1.0): (a) $\theta = 45°$; (b) $\theta = 90°$; (c) $\theta = 135°$. ○, $Re = 1200$; ▲, $Re = 800$; □, $Re = 400$; ●, $Re = 200$; △, $Re = 100$.

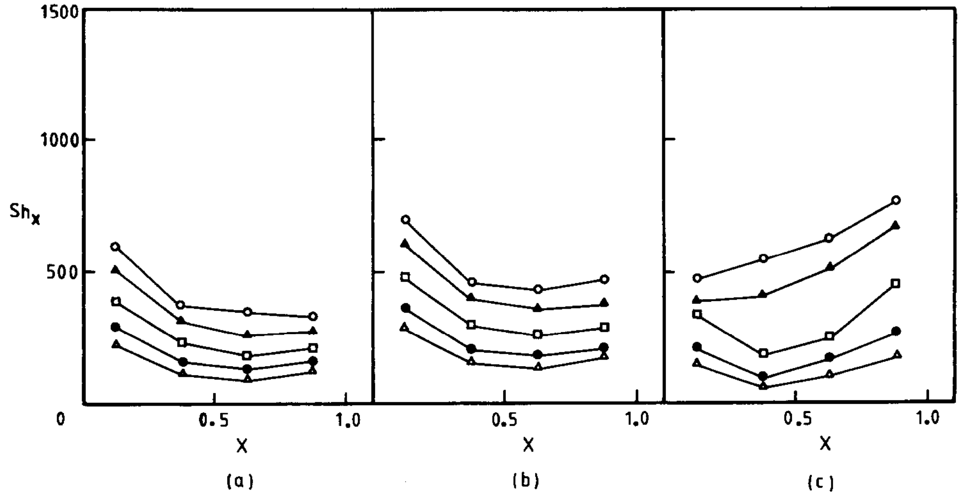

FIG. 11. Local Sherwood number distribution (GP1 = 0.25, GP2 = 0.5): (a) $\theta = 45°$; (b) $\theta = 90°$; (c) $\theta = 135°$.

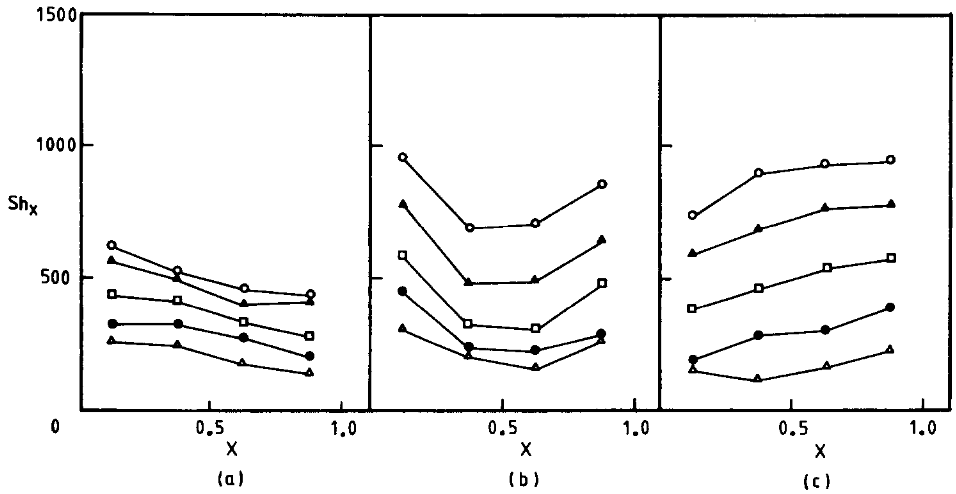

FIG. 12. Local Sherwood number distribution (GP1 = 0.25, GP2 = 2.5): (a) $\theta = 45°$; (b) $\theta = 90°$; (c) $\theta = 135°$. The symbols are the same as in Fig. 4.

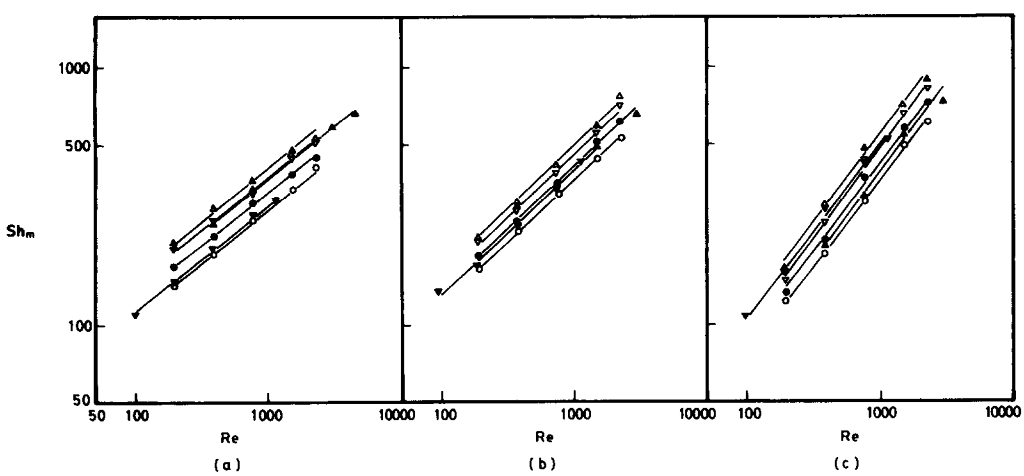

FIG. 13. Effect of Re on mean Sherwood number: (a) $\theta = 45°$, $Re = 100$–4800; (b) $\theta = 90°$, $Re = 100$–3200; (c) $\theta = 135°$, $Re = 100$–3200. ▲, GP1 = 0.125, GP2 = 1.0; ●, GP1 = 0.25, GP2 = 1.0; ▼, GP1 = 0.5, GP2 = 1.0; △, GP1 = 0.25, GP2 = 2.5; ▽, GP1 = 0.25, GP2 = 2.0; ○, GP1 = 0.25, GP2 = 0.5.

alization showed that in the three-dimensional promoter the flow recirculation is not a main mechanism in enhancing the mass transfer, which is different from that in a two-dimensional promoter. The Sherwood number was greatly influenced by the geometry of the flow channel and highly dependent on the Reynolds number as the cross angle increased. The effect of the promoter appeared more strongly as the cross angle increased.

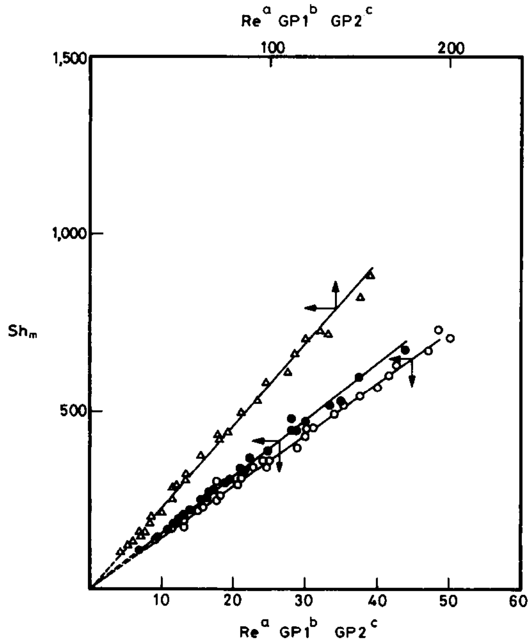

FIG. 14. Correlations of Sh_m vs functions of Re, GP1 and GP2 (Sc = 1650). Range: $\theta = 45°$, Re = 100–4800, ●; $\theta = 90°$, Re = 100–3200, ○; $\theta = 135°$, Re = 100–3200, △; GP1 = 0.125, 0.25 and 0.5; GP2 = 0.5, 1.0, 2.0 and 2.5.

REFERENCES

1. H. Miyashita, A. Takayanagi, Y. Shiomi and K. Wakabayashi, Flow behavior and augmentation of mass transfer rates using a turbulence promoter in rectangular duct, *Kagaku Kogaku Ronbunshu* **6**, 152–156 (1980).
2. J. S. Watson and D. G. Thomas, Forced convection mass transfer: part IV, *A.I.Ch.E. Jl* **13**, 676–677 (1967).
3. A. Solan, Y. Winograd and U. Katz, An analytical model for mass transfer in an electrodialysis cell with spacer of finite mesh, *Desalination* **9**, 89–95 (1971).
4. G. Belfort and G. A. Guter, An experimental study of electrodialysis hydrodynamics, *Desalination* **10**, 221–262 (1972).
5. I. S. Kang and H. N. Chang, The effect of turbulence promoters on mass transfer—numerical analysis and flow visualization, *Int. J. Heat Mass Transfer* **25**, 1167–1181 (1981).
6. D. H. Kim, I. H. Kim and H. N. Chang, Experimental study of mass transfer around a turbulence promoter by limiting current method, *Int. J. Heat Mass Transfer* **26**, 1007–1015 (1983).
7. H. N. Chang and J. K. Park, Effect of turbulence promoter on mass transfer. In *Handbook for Heat and Mass Transfer Operations* (Edited by N. P. Cheremisnoff), Chap. 17. Gulf Publishing, Houston, Texas (1985).
8. P. J. Pickett, *Electrochemical Reactor Design*. Elsevier, New York (1977).
9. J. Newman, *Advances in Electrochemistry and Electrochemical Engineering*, Vol. 5. Wiley, New York (1976).
10. J. K. Aggarwal and L. Talbot, Electrochemical measurements of mass transfer in semi-cylindrical hollows, *Int. J. Heat Mass Transfer* **22**, 61–75 (1979).
11. I. M. Kolthoff and R. Belcher, *Volumetric Analysis*, Vol. III. Interscience, New York (1957).
12. E. J. DeBeer and A. M. Hjort, Employment of potassium ferrocyanide in standardization of dilute potassium permanganate, *Ind. Engng Chem. Analyt. Edn* **7**, 120–121 (1935).
13. K. Torrance, R. Davis, K. Eike, P. Gill, D. Gutman, A. Hsui, S. Lyons and H. Zien, Cavity flows driven by bouyancy and shear, *J. Fluid Mech.* **51**(2), 221–231 (1972).
14. F. Pan and A. Acrivos, Steady flows in rectangular cavities, *J. Fluid Mech.* **28**(4), 643–655 (1967).

TRANSFERT MASSIQUE DANS UN PROMOTEUR DE TURBULENCE TRIDIMENSIONNELLE

Résumé—Le transfert massique local dans un promoteur de turbulence tridimensionnelle est mesuré en utilisant la technique polarographique et l'écoulement est visualisé avec un traçage à l'encre. Le promoteur est un couple de canaux rectangulaires supérieur et inférieur qui se rencontrent avec un angle donné pour former une région de mélange pour les deux couches de courant de fluide venant de chaque canal. Les flux de transfert massique locaux et globaux sur 16 électrodes segmentées sont mesurés pour étudier les effets du nombre de Reynolds (*Re*) et le rapport des deux vitesses moyennes dans les canaux en faisant varier l'angle de croisement et le rapport hauteur-largeur du canal. La plus grande efficacité de croisement de 135° et elle est progessivement moindre avec 90° et 45°. La visualisation de l'écoulement montre qu'avec le promoteur tridimensionnel, un tourbillon crée par les deux courants croisés interfaciaux est le mécanisme principal qui casse une couche limite de concentration, en contradiction avec les écoulements de recirculation dans les promoteurs bidimensionnels étudiés par Chang et ses collaborateurs (1983, 1984).

STOFFÜBERTRAGUNG IN EINEM DREIDIMENSIONALEN NETZFÖRMIGEN TURBULENZPROMOTOR

Zusammenfassung—Es wurden örtliche Stoffübergangsgeschwindigkeiten in einem dreidimensionalen netzförmigen Turbulenzpromotor gemessen, wobei ein elektrochemisches Diffusionsgrenzstromverfahren angewandt wurde und das Strömungsmuster mit einem Tintenspurinjektor sichtbar gemacht wurde. Der Modellpromotor bestand aus einem oberen und einem unteren rechteckigen Strömungskanal, die sich in einem vorgegebenen Winkel überlappten, um eine Grenzflächenkontakt- und Mischregion für die beiden Fluidschichten, die aus jedem Kanal kamen, zu bilden. Örtliche und mittlere Stoffübertragungsgeschwindigkeiten wurden mit 16 segmentierten Elektroden gemessen, um den Einfluß der Reynoldszahl (*Re*) und das Verhältnis von zwei mittleren Geschwindigkeiten im oberen und unteren Kanal bei verschiedenen Kreuzstromwinkeln und Höhe/Breite-Verhältnissen zu untersuchen. Die höchsten Mischungsgrade wurden im Promotor bei einem Kreuzstromwinkel von 135° erhalten, dagegen zunehmend weniger bei solchen zwischen 90° und 45°. Die Sichtbarmachung der Strömung zeigte, daß im dreidimensionalen Promotor durch die beiden Kreuzströme ein Wirbel entstand, der die Hauptursache für das Aufbrechen der Konzentrationsgrenzschicht war, im Gegensatz zu den rezirkulierenden Strömungen, die Chang und Mitarbeiter in zweidimensionalen Promotoren untersuchten.

МАССОПЕРЕНОС В ТРЕХМЕРНОМ ТУРБУЛИЗАТОРЕ СЕТЧАТОГО ТИПА

Аннотация—Интенсивности локального массопереноса в трехмерном турбулизаторе измерялись методом предельного тока. Визуализация течения осуществлялась с помощью чернильного трассера. Модельный турбулизатор состоял из верхнего и нижнего прямоугольных каналов, которые пересекались под заданным углом с целью формирования зоны смешения двух потоков жидкости, протекающих через каждый канал. Для изучения влияния числа Рейнольдса (*Re*) и отношения средних скоростей потоков в верхнем и нижнем каналах с помощью 16 разделенных на сегменты электродов измерялись интенсивности локального и интегрального массообмена при изменении угла пересечения потоков и отношения высоты каналов к ширине. Наибольшая эффективность смешения получена в турбулизаторе с углом пересечения потоков, равным 135°, и существенно меньшая—при углах 90 и 45°. Визуализация течения показала, что, в отличие от рециркуляционных течений в двумерных турбулизаторах, исследованных Ченгом с сотрудниками (1983, 1984), вихрь, образованный двумя пересекающимися потоками в трехмерном турбулизаторе, в основном определяет механизм разрушения концентрационного пограничного слоя.